BIOCHEMISTRY
including biophysical chemistry & molecular biology

Article

pubs.acs.org/biochemistry

Kinetically and Crystallographically Guided Mutations of a Benzoate CoA Ligase (BadA) Elucidate Mechanism and Expand Substrate Permissivity

Chelsea K. Thornburg,[‡] Susan Wortas-Strom,[†] Meisam Nosrati,[†] James H. Geiger,[*,†] and Kevin D. Walker[*,‡,†]

[†]Department of Chemistry, Michigan State University, East Lansing, Michigan 48824, United States

[‡]Department of Biochemistry and Molecular Biology, Michigan State University, East Lansing, Michigan 48824, United States

Supporting Information

ABSTRACT: A benzoate CoA ligase (BadA), isolated from the bacterium *Rhodopseudomonas palustris*, catalyzes the conversion of benzoate to benzoyl CoA on the catabolic pathway of aromatic carboxylic acids. Herein, apparent Michaelis constants k_{cat}^{app} and K_M^{app} were determined for an expanded array of 31 substrates chosen to systematically probe the active site architecture of the enzyme and provide a baseline for expansion of wild-type substrate specificity. Acyl CoA products were observed for 25 of the 31 substrates; in general, BadA converted *ortho*-substituted substrates better than the corresponding *meta* and *para* regioisomers, and the turnover number was more affected by steric rather than electronic effects. The kinetic data are interpreted in relation to six crystal structures of BadA in complex with several substrates and a benzoyl-AMP reaction intermediate. In contrast to other known natural substrate-bound benzoate ligase structures, all substrate-bound BadA structures adopted the thiolation conformation instead of the adenylation conformation. We also observed all the aryl carboxylates to be uniquely oriented within the active site, relative to other structures. Together, the kinetics and structural data suggested a mechanism that involves substrate binding in the thiolation conformation, followed by substrate rotation to an active orientation upon the transition to the adenylation conformation. On the basis of this hypothesis and the structural data, sterically demanding active site residues were mutated, and the substrate specificity was expanded substantially versus that of BadA. Novel activities were seen for substrates with larger substituents, including phenyl acetate. Additionally, the mutant Lys427Ala identified this nonconserved residue as essential for the thiolation step of BadA, but not adenylation. These variously acylated CoAs can serve as novel substrates of acyl CoA-dependent acyltransferases in coupled enzyme assays to produce analogues of bioactive natural products.

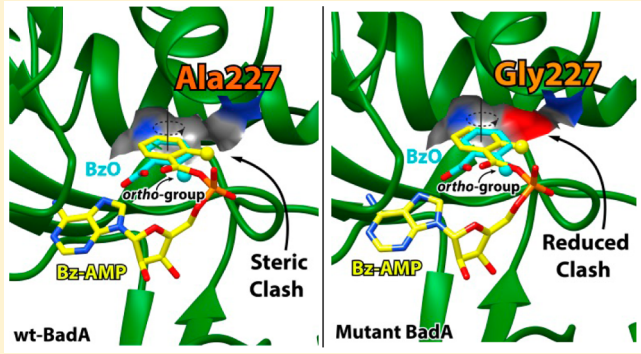

Acyl-group adenylation by ATP, in both primary and specialized metabolism, is common to all living organisms. The superfamily of ATP-dependent adenylation enzymes (PFAM00501) is organized into three classes.[1] Class I includes the nonribosomal peptide synthetase (NRPS) adenylation domains, the acyl CoA ligases, and luciferase oxidoreductases.[2] Classes II and III comprise the aminoacyl-tRNA synthetases and NRPS-independent siderophore (NIS) enzymes, respectively.[3] The focus of the study presented here centers on an acyl CoA ligase from class I. Plants and bacteria employ aroyl CoA thioesters for the biosynthesis of specialized metabolites. For example, anthraniloyl CoA is a precursor of a quorum-sensing molecule in *Pseudomonas aeruginosa*;[4] benzoyl CoA lies on the pathway to enterocin (a bacteriocin) in the marine actinomycete *Salinispora*,[5] to the chemotherapeutic Taxol in *Taxus* plants,[6,7] and to the volatile fragrant benzylbenzoate in plants.[8] Biosynthesis of the antibacterial and antifungal aureothin proceeds through 4-nitrobenzoyl CoA in the soil bacterium *Streptomyces thioluteus* (Figure 1).[9,10]

Accounts of aerobic and anaerobic degradation of environmental pollutants such as polycyclic aromatic hydrocarbons (PAHs) and polychlorinated biphenyls (PCBs) to benzoate derivatives in bacteria include the characterization of several different aroyl CoA ligases from *Rhodopseudomonas palustris*, *Burkholderia xenoverans*, *Pseudomonas* strain CBS3, *Thauera aromatica*, and *P. aeruginosa*.[11−16] Redox enzymes in these bacteria target the aroyl CoA thioesters for dearomatization and ring cleavage along catabolic pathways.[17,18] These organisms are thus candidates for bioremediation of man-made PAHs and PCBs to reduce their environmental impact.[17,19]

Received: August 13, 2015
Revised: September 15, 2015
Published: September 17, 2015

DOI: 10.1021/acs.biochem.5b00899
Biochemistry 2015, 54, 6230−6242

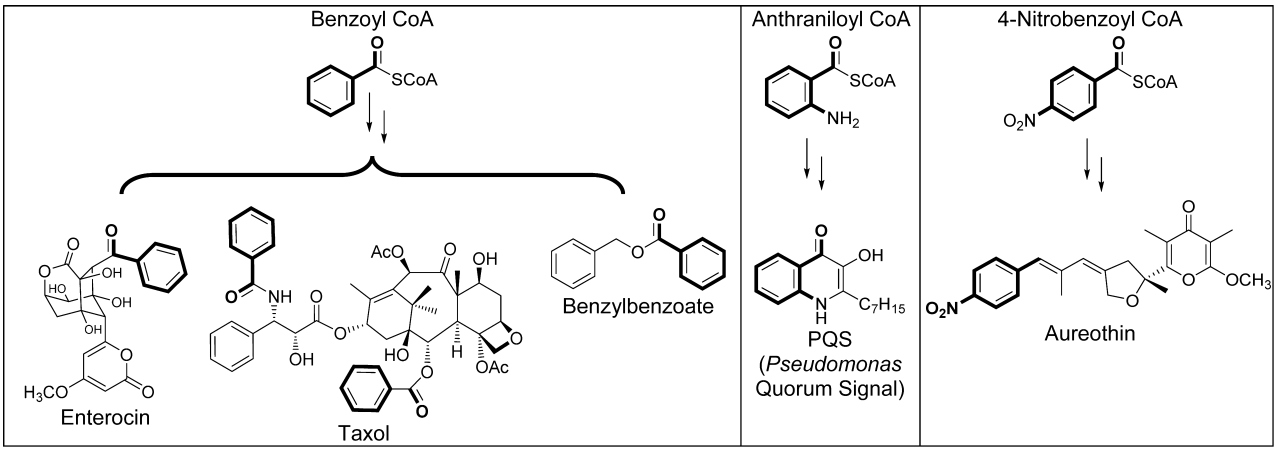

Figure 1. Representative natural products derived from acyl CoA thioesters.

ATP-dependent CoA ligases use two half-reactions to catalyze thioesterification (Figure 2).[20] The enzyme binds an alkyl or aryl carboxylate and a Mg^{2+}−ATP complex for subsequent coupling during the first half-reaction. The oxyanion of the carboxylate nucleophilically attacks ATP, releases diphosphate, and forms an acyl-AMP mixed anhydride intermediate. In the second half-reaction, the nucleophilic thiol of CoA attacks the carbonyl of the acyl-AMP intermediate to make the thioester. Other crystal structures from this ligase family support the hypothesis that the enzymes adopt adenylation and thiolation conformations to catalyze their respective half-reactions.[15,21,22]

Several active aroyl CoA ligase structures have been determined in complex with acyl carboxylates, cofactors, acyl-

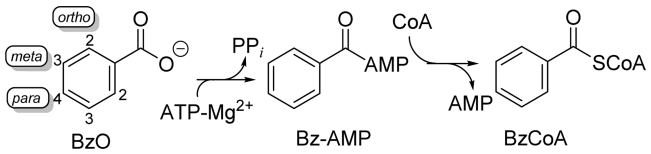

Figure 2. ATP-dependent, two-step mechanism of a benzoate:CoA ligase in the presence of magnesium. Abbreviations: BzO, benzoate; Bz-AMP, benzoyl AMP; BzCoA, benzoyl coenzyme A. The *ortho*, *meta*, and *para* carbons of the aryl ring of BzO are highlighted with carbon numbers 2, 3, and 4, respectively.

adenylates, AMP, ATP, and CoA.[14,15,21,23−29] *R. palustris*, chosen as a potential bacterial candidate for bioremediation, has at least three distinct aroyl CoA ligases with different substrate specificities and regulatory characteristics.[13,30] Of these, a benzoate CoA ligase (designated BadA) was identified in an earlier study[12] that reported on the relative V_{max} (i.e., V_{rel}) values of BadA for different substrates compared to benzoate.[12] Here, we explicitly calculated the apparent kinetic parameters (k_{cat}^{app} and K_M^{app}) of BadA for 25 different carboxylate substrates to further understand the steric, mesomeric, and inductive effects of the substituents on the mechanism. We intend to repurpose BadA for use in coupled enzyme assays to biosynthesize rare, non-natural acyl CoAs. These thioesters will serve as substrates for CoA-dependent *N*- and *O*-acyltransferases that acylate many bioactive specialized metabolites from plants.[31,32] Calculation of the intrinsic catalytic constants of BadA for non-natural carboxylates is an important step toward this goal.

Also described herein are five X-ray crystal structures of recombinant BadA at ∼1.80 Å resolution complexed with various aryl carboxylates and one with benzoyl-AMP (Bz-AMP). BadA is structurally similar to other CoA ligases in its class, comprising separate N-terminal and C-terminal domains joined by a flexible hinge. On the basis of the structures of other aroyl CoA ligases, we expected the C-terminal domain of BadA−carboxylate complexes to remain in an "unrotated" adenylate-forming conformation as seen in other benzoate derivatives in complex with ligases.[21,23,27] Surprisingly, however, each complex showed BadA in the conformation primed for thioesterification. The homologous human medium chain fatty acyl CoA synthetase (ACSM2A)[24] provides precedent for the binding of benzoate (BzO) to BadA in the thiolation conformation. By analogy, ACSM2A cocrystallized with the surrogate substrate ibuprofen in the thiolation conformation.[24] In addition, each of the aryl carboxylates binds the BadA active site in a unique configuration rotated ∼60° about the phenyl ring relative to BzO bound in other structures and the Bz-AMP bound in BadA. Here, mutagenesis of the active site supports the importance of both orientations of the substrate in the active site. Together, the data support a mechanism in which benzoate tightly binds BadA in the thiolation conformation, followed by rotation in the active site upon ATP binding for the acyl adenylation step. The structures further provide a basis for rational mutagenesis to remove sterically challenging residues from the active site and expand the substrate scope of BadA. The results of a series of mutations are also described here. Using these structures, we also determined that the non-conserved active site Lys427, present in the BadA active site in the thiolation conformation, is not required for acyl adenylate formation but is necessary for thioesterification.

■ MATERIALS AND METHODS

BadA Protein Expression and Purification. The *pBadA* expression vector (pET28a+) was used to transform BL21-(DE3) *Escherichia coli* (Invitrogen, Carlsbad, CA). A single colony was selected and used to inoculate a 10 mL culture of Luria-Bertani (LB) medium (Acumedia) containing 50 μg/mL kanamycin (Roche Life Sciences, Indianapolis, IN). The culture was grown overnight at 37 °C. This seed culture (5 mL) was used to inoculate fresh LB medium (1 L) containing 50 μg/mL kanamycin. This culture was grown at 37 °C until the A_{600} reached 0.8. Gene expression was induced by 0.5 mM isopropyl β-D-1-thiogalactopyranoside, and the cultures were grown for 5

DOI: 10.1021/acs.biochem.5b00899
Biochemistry 2015, 54, 6230−6242

h at 18 °C and harvested by centrifugation at 6000*g*. The bacterial pellet was resuspended in buffer A [50 mM Na_2PO_4, 300 mM NaCl, 15 mM imidazole, and 5% glycerol (pH 8.0)] containing EDTA-free Protease Inhibitor Cocktail tablets (Roche Life Sciences, Indianapolis, IN). Cells were lysed with a Misonix XL 2020 sonicator and centrifuged at 18000*g* for 30 min. The supernatant was passed through a 0.2 μm filter (Millipore, Billerica, MA) and loaded onto a Ni^{2+}-NTA Qiagen column pre-equilibrated with buffer A. The column was washed with 5 column volumes (CV) of buffer A and eluted with 3 CV of buffer A containing 250 mM imidazole. Each fraction was analyzed by sodium dodecyl sulfate−polyacrylamide gel electrophoresis. Fractions containing BadA were combined, loaded into a 10 kDa MW cutoff dialysis cassette (Thermo Scientific Pierce, Grand Island, NY), and dialyzed overnight against buffer B [50 mM $NaPO_4$ containing 5% glycerol (pH 8.0)] for kinetic analysis or buffer C [20 mM Tris (pH 8.0)] for protein crystallization experiments. Dialyzed protein was concentrated in a Millipore Amicon Ultra 30 kDa cutoff concentrator to ∼10 mg/mL [estimated by the Coomassie (Bradford) Protein Assays (Thermo Scientific Pierce)]. The molecular weight of BadA (501 amino acids, 58.9 kDa) was verified by liquid chromatography and mass spectrometry (LC−ESI/MS) on a Q-ToF Ultima Global mass spectrometer (Waters Corp., Milford, MA). Protein aliquots were frozen in liquid nitrogen and stored at −80 °C.

BadA Kinetic Assays. Stocks of ATP (10 mM) and CoA (10 mM) were dissolved in buffer B; $MgCl_2$ (at 100 mM) was stored in water, and stocks of the aromatic carboxylic acids (each at 100 mM) were dissolved in methanol. Aromatic carboxylic acids were then diluted in water. To establish steady-state kinetic rates of BadA with respect to protein concentration and time for each carboxylate (1 μM to 4 mM) and other reactants, ATP (250 μM), CoA (250 μM), and $MgCl_2$ (750 μM) were combined in buffer B and preincubated at 31 °C for 10 min before the addition of 0.1−20 μg/mL BadA (total volume of 90 μL). Assays were acid-quenched (pH 3) with 8.8% formic acid in water. Acetyl CoA was added as an internal standard at a final concentration of 1 μM. Methanol concentrations were held constant at 1% (v/v) among assays with varied concentrations of carboxylic acids.

BadA Assay Analysis by Liquid Chromatography and Mass Spectrometry. Liquid chromatography and electrospray tandem mass spectrometry (LC−ESI/MS/MS) in negative ion mode was used to quantify the biosynthetic acyl CoA products. An autosampler (at 10 °C) connected to a UPLC system (Waters Corp.) injected a 10 μL aliquot of each assay onto an Ascentis Express C18 HPLC column (2.7 μm, 5 cm × 2.1 mm, at 30 °C, Sigma-Aldrich). The column was eluted at 0.4 mL/min with 2.5% solvent B (100% acetonitrile) and 97.5% solvent A [0.05% triethanolamine in water (pH 5.5)] with a 0.5 min hold, followed by a linear gradient to 20% solvent B over 4 min, then increased to 100% solvent B over 2 min, and finally lowered to 2.5% solvent B over 0.5 min. The needle was washed with 2 mL each of 100% 2-propanol and then with 10% acetonitrile in water prior to each injection. The HPLC effluent was directed to an electrospray ionization mass spectrometer (Quattro Premier XL, Waters Corp.) in negative ion mode, with a cone voltage of 60 eV and a collision energy of 44 eV. Each aryl CoA was quantified by multiple-reaction monitoring of the $[M - H]^- \rightarrow m/z$ 408 transition, common to each aryl CoA tested (Figure 3). Peak areas (calculated using the MassLynx data analysis software from Waters Corp.) were converted to product concentrations using a standard curve for a series of benzoyl CoA concentrations [61 nM to 15.6 μM (n = 3)] that were corrected by an internal standard acetyl CoA (1 μM).

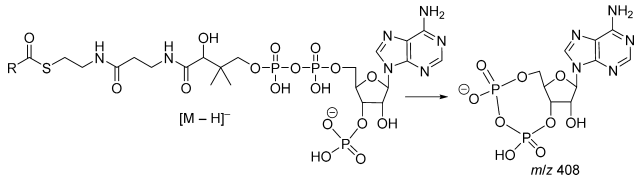

Figure 3. Multiple-reaction monitoring (MRM) LC−ESI/MS/MS of the $[M - H]^- \rightarrow m/z$ 408 transition ion in negative ion mode for aryl CoA thioesters.

BadA Mutations. Point mutations of the *badA* gene were generated by site-directed mutagenesis, using the following forward and reverse primer pairs (mutated bases are underlined): A227G, 5′-CCA AAC TGT TTT TCG GCT ACG GCC TCG GCA ACG-3′ and 5′-CGT TGC CGA GGC CGT AGC CGA AAA ACA GTT TGG-3′; L333A, 5′-CGG CTC GAC CGA GAT GGC GCA CAT CTT TCT GTC GAA C-3′ and 5′-GTT CGA CAG AAA GAT GTG CGC CAT CTC GGT CGA GCC G-3′; H334A, 5′-CGG CTC GAC CGA GAT GCT GGC GAT CTT CCT GTC GAA TTT G-3′ and 5′-CAA ATT CGA CAG GAA GAT CGC CAG CAT CTC GGT CGA GCC G-3′; I335A, 5′-CCG AGA TGC TGC ACG CGT TTC TGT CGA ACC TGC-3′ and 5′-GCA GGT TCG ACA GAA ACG CGT GCA GCA TCT CGG-3′; K427A, 5′-CGA CAT GCT GGC GGT CAG CGG CAT CTA TGT CAG CCC GTT CGA GAT CG-3′ and 5′-GCC GCT GAC CGC CAG CAT GTC GTC GGT GCG GCC CGC ATA GGT GTA G-3′. The pBadA plasmid was amplified via polymerase chain reaction (PCR) using Phusion HF polymerase (New England Biolabs, Ipswich, MA) under the following protocol: 95 °C for 3 min, followed by 20 cycles of 95 °C for 1 min, 58 °C for 1 min, and 72 °C for 4.5 min, with a final elongation step of 72 °C for 7 min. The PCR product was digested with DpnI (New England Biolabs) at 37 °C for 2 h and then used to transform DH5α *E. coli* (Invitrogen). The resulting colonies were inoculated into starter cultures and grown for DNA purification (PureYield Plasmid MiniPrep System, Promega, Fitchburg, WI) and DNA sequencing for the *badA* point mutations at the Michigan State University Research Technology Support Facility. Mutant plasmids were used to transform BL21(DE3) *E. coli* (Invitrogen). The expression, isolation, and purification of the mutant enzyme were identical to those processes described for wild-type BadA.

Kinetic Analysis. To calculate the kinetic constants, each substrate was varied (1−4000 μM) in separate assays under predetermined steady-state conditions. Resultant CoA thioester products were quantified after terminating the reaction as described previously. The apparent kinetic parameters (K_M^{app} and k_{cat}^{app}) were calculated by nonlinear regression with Origin Pro version 9.0 (Northampton, MA) (Figures S1−S24 of the Supporting Information), using the Michaelis−Menten equation: $v_0 = k_{cat}^{app}[E_o][S]/(K_M^{app} + [S])$. Relative steady-state rates for mutant enzymes Ala227Gly-BadA, Leu332Ala-BadA, His333Ala-BadA, and Ile334Ala-BadA were calculated for 15 aryl carboxylates. Assays with purified mutant protein contained 0.02 mg/mL mutant enzyme, 250 μM ATP, 1 mM carboxylate, 750 μM Mg^{2+}, and 250 μM CoA. Relative velocities at apparent saturation are reported as percentages relative to BadA with

DOI: 10.1021/acs.biochem.5b00899
Biochemistry 2015, 54, 6230−6242

benzoate. For the Lys427Ala-BadA mutant, the biosynthetic benzoyl-AMP and benzoyl CoA products catalyzed by the mutant were analyzed separately via HPLC (with A_{254} detection) and LC−ESI-MS/MS. Control assays contained the necessary cofactors and reagents but no mutant enzyme.

Crystallization of *R. palustris* Benzoate: Coenzyme A Ligase (BadA). Purified BadA protein (17.5 mg/mL) was used for *de novo* protein crystallization trials using six different 96-condition Crystal Screen (Hampton Research) matrices. A Gryphon Protein Crystallization robot (Art Robbins Instruments) was used for setting up sitting-drop vapor diffusion crystallization trials. The trials were kept at 22 °C throughout crystallization. Approximately 45 different conditions produced crystals of varying quality, the best being from the Wizard I/II Screen A10 condition [20% (w/v) PEG-2000 MME and 0.1 M Tris-HCl (pH 7)]. This condition was then optimized in crystal boxes employing the hanging-drop vapor diffusion crystallization method. Hanging drops (2 μL) consisting of an equal measure of protein and reservoir solutions were used. The best crystals, used for data collection, were grown from a reservoir solution containing 0.1 M Tris-HCl (pH 7.0) and 15% (w/v) PEG 3350.

Cocrystallization To Obtain the Ligand-Bound Structure. Cocrystallization was employed by adding separately each carboxylic acid ligand (4 equiv) to the BadA protein solubilized in 0.1 M Tris buffer (pH 8.0). For the multiple-component cocrystallization, ATP, CoA, and benzoic acid (each at 1 equiv) were added to the protein solution. Each cocrystallization mixture was incubated for 10 min at 4 °C followed by crystallization using a reservoir of 20 mM Tris buffer at 15% PEG 3350 at variable pH values. The best crystals grew in a pH range from 6.5 to 7.5.

Data Processing and Refinement of BadA. Crystals were soaked in a cryoprotectant [0.2 M Tris-HCl (pH 6.5−7.5) containing 20% PEG-3350 and 20% glycerol], mounted in CryoLoops (Hampton Research), and then flash-frozen in liquid nitrogen. The native X-ray diffraction intensity data were collected under a continuous stream of nitrogen at 100 K on beamline 21-ID-G (LS-CAT, Argonne National Laboratory, Advanced Photon Source, Chicago, IL) at a wavelength of 0.97872 Å. Raw diffraction data were indexed using the HKL2000 software package.[33] A search of the Research Collaboratory for Structural Bioinformatics (RCSB) Protein Data Bank (PDB) revealed one known structure for a benzoate CoA ligase (BCL_M) from *Burkholderia xenovorans* LB400 (PDB entry 2V7B).[14] Query of the Swiss-Model server[34] produced a threaded protein structure homology model of BadA based on the BCL_M structure. The BadA structure was determined by molecular replacement using this model and the MOLREP program in the CCP4 suite.[35−37] Though the N-terminal domain was well-positioned within the density, the C-terminal domain was not. The model was corrected using the Buccaneer program in the CCP4 suite to thread the amino acid sequence into the density. Further corrections were made manually using COOT.[38] Jligand version 1.0.9[39] of the CCP4 suite was used to add the template restraints for the ligands prior to refinement. The structures were refined using REFMAC in the CCP4 program suite. Water molecules were added using REFMAC and COOT near the end of the refinement.

Calculation of Covalent van der Waals Volumes and Lengths. The molecular volumes of the substituents on the aryl carboxylate substrates were estimated as Connolly solvent-excluded volumes[40] using ChemBio3D Ultra software (version 13.0, PerkinElmer) and a probe radius of 0.1 Å. The volume of a phenyl anion was subtracted from the estimated volume of a phenyl attached to a substituent. The geometries of polyatomic substituents such as CH_3, OH, MeO, CN, NH_2, and NO_2, attached to phenyl were MM2 energy minimized using the default parameters of the ChemBio3D Ultra software. The covalent van der Waals lengths of CN and Cl substituents attached to a phenyl ring were calculated using the covalent bond distance between two atoms and the atomic radius of the terminal atom.

RESULTS

Determining the BadA Structure. BadA crystallized as a complex with benzoate (BzO) in the absence of added benzoate. BadA also cocrystallized with 2-fluorobenzoate (2-F-BzO), 2-methylbenzoate (2-Me-BzO), 3-furoate (3-Fur), and thiophene-2-carboxylate (Thio-2-C) (see Figure 2 and Figures S1−S24 for structures). BadA was also cocrystallized with both benzoate and ATP, resulting in a bound Bz-AMP intermediate, the product of the first half-reaction (see Figure 2), bound in the active site. All structures were refined to resolutions of at least 1.8 Å (Table S1 of the Supporting Information) and helped guide the interpretation of the kinetic data.

Domain Orientation. The BadA structures in complex with BzO (PDB entry 4EAT) (Figure 4 and Figure S25), 2-Me-BzO (PDB entry 4RLQ), Thio-2-C (PDB entry 4RMN), 3-Fur (PDB entry 4RM3), 2-F-BzO (PDB entry 4RM2), and Bz-AMP (PDB entry 4ZJZ) (Figure S26 of the Supporting Information) had the characteristic N-terminal and C-terminal domains of other ATP-dependent adenylases.[2,28] The N-terminal (residues 1−434) and C-terminal (residues 435−522) domains of BadA fold analogously to the benzoate CoA ligase BCL_M (PDB entry 2V7B)[14] with root-mean-square deviations between the peptide backbones of ∼0.5 and 0.6 Å, respectively.[41] The N-terminal domain contains the benzoate binding site, and the C-terminal domain contacts the outer edge of the benzoate binding pocket, positioning benzoate in the active site through a charged interaction between the carboxylate of benzoate and Lys427 (Figure 4).

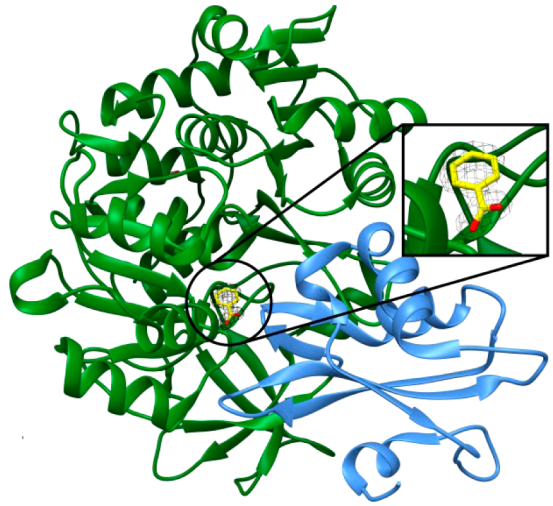

Figure 4. Crystal structure of BadA (PDB entry 4EAT) in complex with benzoate (yellow and enclosed in the electron density map, $2F_o - F_c$). The N-terminal domain (green) and the C-terminal domain (blue) in the "thiolation conformation".

DOI: 10.1021/acs.biochem.5b00899
Biochemistry 2015, 54, 6230−6242

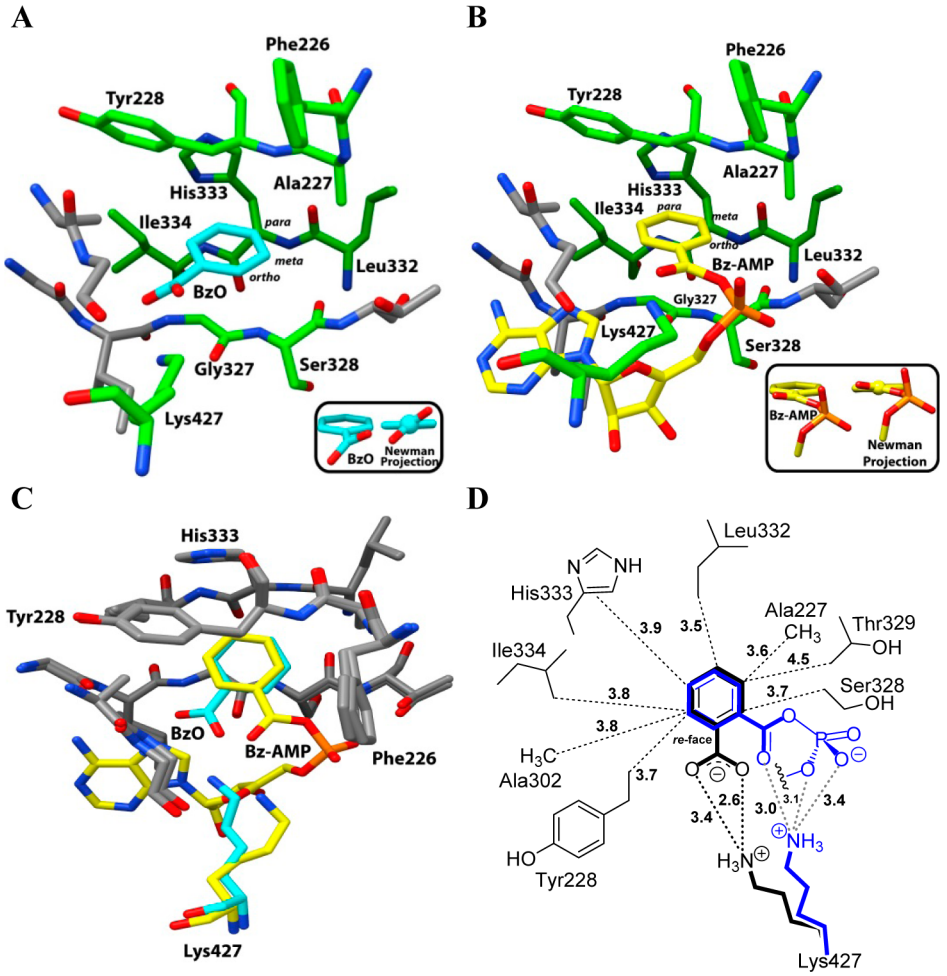

Figure 5. Active site of the BadA structure. (A) Three-dimensional rendering of BadA in complex with benzoate (BzO) (cyan) (PDB entry 4EAT) and (B) benzoyl-AMP (Bz-AMP) (yellow) (PDB entry 4ZJZ); key, steric, and substrate binding residues (green) are highlighted. (C) Overlay of the active site orientations of BzO (cyan) and Bz-AMP (yellow) in complex with BadA. Structural alignments were made with UCSF Chimera 1.10.[42] (D) Two-dimensional rendering of the active site showing distances (in angstroms) between BzO (bold black structure) and the Bz group of Bz-AMP (bold blue structure) and key, steric active site residues. Insets show two views of the dihedral angle between the carboxylate oxygens and the phenyl ring of BzO and Bz-AMP (partial structure) bound in BadA. Heteroatoms are colored red for oxygen, orange for phosphorus, and blue for nitrogen.

Features of the BadA Active Site. The BadA active site is largely hydrophobic with many binding contacts between the substrate and the polypeptide backbone. In all BadA structures bound to the aryl carboxylate, the active site coordinates the carboxylate substrate with Lys427. In this position, the *para* carbon of BzO neighbors the carbonyl of Leu332 along the peptide backbone, and the two *meta* carbons of BzO point toward His333 and Ala227 on either side (Figure 5A,D). The *si*- and *re*-faces of the BzO are positioned between backbone amide bonds comprising Gly327, Ser328, and Thr329 on one face and Tyr228 on the other face.

Cocrystallization of BadA with BzO and ATP yielded a Bz-AMP intermediate in the active site with the C-terminal domain also poised in the thiolation conformation.[21,26] The active sites of structures bound to BzO or Bz-AMP showed almost no structural differences. However, when Bz-AMP forms, Lys427 moves from an interaction with the carboxylate of the substrate to several polar contacts with the Bz-AMP and the peptide backbone (Figure 5B,D). We evaluated the importance of Lys427 of BadA for catalysis by making a Lys427Ala-BadA mutant and compared its activity with that of BadA. The mutant made benzoyl CoA at a rate [k_{cat}^{app} = (83 ± 1.8) × 10^{-5} s^{-1}] more than 33000-fold slower than that of wild-type BadA (k_{cat}^{app} = 28 s^{-1}), yet the K_M^{app} (1.5 ± 0.31 μM) for this mutant was nearly the same for wild-type BadA (4.4 ± 0.65 μM) (Figure S27). The mutant and BadA catalyzed approximately equal amounts of benzoyl-AMP in the absence of CoA (Figure S28). These data indicated that Lys427 is needed for the thiolation reaction.

When the Bz-AMP anhydride forms, other structural differences include a decrease in the dihedral angle between the carboxylate and the aryl ring from 37° for BzO to 12° for the anhydride. Further, Tyr432 shifted toward the phosphate oxygen of the AMP anhydride and away from Arg421 to accommodate the Bz-AMP (Figure S27). The benzoyl moiety also rotates ~60° about the C_6 axis of the aromatic ring and moves the *ortho* carbon from an unhindered region of the active site toward residue Ala227, which previously resided near the *meta* carbon (Figure 5C,D). This rotation positions the benzoyl moiety of Bz-AMP similarly to those of benzoates bound in other CoA ligase structures, regardless of the C-terminal domain orientation.[14,21,23]

Kinetic Properties of BadA. The *R. palustris* BadA was recombinantly overexpressed in *E. coli* and incubated separately

DOI: 10.1021/acs.biochem.5b00899
Biochemistry 2015, 54, 6230−6242

with various heteroaromatic, alkenoyl, alkyl, and aryl carboxylates to calculate the kinetic constants for each substrate (Table 1). Benzoate substrates with substituents of differing steric and electronic properties were chosen to systematically probe the active site of BadA. We quantified the biosynthetic CoA thioester products by LC−ESI-MS/MS.

Table 1. Kinetic Parameters of BadA for Various Substrates

substrate[a]	k_{cat}^{app} (s^{-1})	K_M^{app} (μM)	k_{cat}^{app}/K_M^{app} (s^{-1} μM^{-1})
BzO	28 ± 0.9	4.4 ± 0.65	6.4
Thio-2-C	4.8 ± 0.2	37 ± 5.7	0.13
3-Fur	6.7 ± 0.5	71 ± 12	0.094
PhAc	ND[b]	–	–
Cinn	ND[b]	–	–
Nonaromatic Carboxylates			
3-Cyc	16 ± 1.03	56 ± 9.1	0.29
1-Cyc	5.6 ± 0.24	52 ± 7.1	0.11
Cyc	13.5 ± 1.07	1470 ± 213	0.0092
ortho-Substituted Benzoates			
2-F	34 ± 0.7	8.1 ± 0.91	4.2
2-OH	0.63 ± 0.01	1.6 ± 0.2	0.39
2-NH_2	3.9 ± 0.12	21 ± 2.3	0.19
2-CN	0.11 ± 0.0034	213 ± 22	0.00052
2-Cl	2.2 ± 0.07	130 ± 12	0.017
2-Me	1.2 ± 0.042	44 ± 6.1	0.027
2-MeO	0.011 ± 0.0005	789 ± 82	0.000014
2-NO_2	0.27 ± 0.011	2015 ± 167	0.00013
meta-Substituted Benzoates			
3-F	35 ± 1.4	73 ± 11	0.48
3-OH	1.8 ± 0.04	229 ± 18	0.0079
3-NH_2	1.8 ± 0.11	174 ± 32	0.010
3-CN	slow[c]	–	–
3-Cl	0.33 ± 0.01	290 ± 23	0.0011
3-Me	0.54 ± 0.018	215 ± 26	0.0025
3-MeO	ND[b]	–	–
3-NO_2	ND[b]	–	–
para-Substituted Benzoates			
4-F	22 ± 0.66	6.6 ± 0.9	3.3
4-OH	0.93 ± 0.037	158 ± 17	0.0059
4-NH_2	0.18 ± 0.004	25 ± 3	0.0072
4-CN	slow[c]	–	–
4-Cl	0.29 ± 0.012	83 ± 11	0.0035
4-Me	0.7 ± 0.035	590 ± 73	0.0012
4-MeO	ND[b]	–	–
4-NO_2	ND[b]	–	–

[a]Abbreviations: Thio-2-C, thiophene-2-carboxylate; 3-Fur, 3-furoate; PhAc, phenylacetate; Cinn, cinnamate; 3-Cyc, 3-cyclohexene-carboxylate; 1-Cyc, 1-cyclohexene-carboxlyate; Cyc, cyclohexane carboxylate. Standard errors were calculated for the nonlinear regression fit by Origin Pro version 9.0. [b]Not detectable, below the detection limit. [c]The CoA thioester product was detected at 0.4 pmol s^{-1} at apparent saturation, even at BadA concentrations up to 100 ug/mL. Initial steady-state rates at low substrate concentrations were too slow to calculate kinetic parameters.

Substrate Turnover by BadA. The k_{cat}^{app} (28 ± 0.9 s^{-1}) and K_M^{app} (4.4 ± 0.65 μM) of BadA for the natural substrate BzO are consistent with those reported earlier (k_{cat}^{app} = 27 s^{-1}; K_M^{app} = 0.6−2 μM).[12] These values were compared to the Michaelis parameters of BadA for 21 monosubstituted benzoates, three cyclohexane-derived carboxylates, and two heteroaromatic carboxylates to their corresponding CoA thioesters (Table 1). Although K_M is not a true dissociation constant, in this study it will serve as a means of comparing enzyme interactions with different carboxylate substrates.

Halogenated Benzoates. BadA turned over substrates 2-F-, 3-F-, and 4-F-BzO as well as BzO, and the K_M^{app} values of BadA for 2-F-BzO and 4-F-BzO were similar to that for BzO; 3-F-BzO was an outlier (Table 1). Interestingly, the K_M^{app} for 3-F-BzO was 17-fold higher than for BzO, reducing its relative catalytic efficiency 13-fold and suggesting that an interaction between the *meta* position and active site residues affected binding but not turnover.

BadA turned over 2-chlorobenzoate (2-Cl-BzO) better than 3-Cl-BzO or 4-Cl-BzO, in a trend similar to that of the fluorobenzoates. However, compared to that of BzO, turnover rates were ∼10-fold slower for 2-Cl-BzO and 100-fold slower for both 3-Cl- and 4-Cl-BzO. The K_M^{app} values of BadA for the Cl-BzO series (between 83 and 290 μM) were much higher than those of the corresponding F-BzO substrates (<10 μM). Accordingly, the k_{cat}^{app}/K_M^{app} values of BadA for the Cl-BzO substrates were considerably reduced (∼380-fold for 2-Cl-BzO and up to ∼6000-fold for 3-Cl-BzO) compared to that for BzO. These data suggest the larger chlorine[43] likely affects the binding interaction of all regioisomers of the chlorinated substrates and prevents them from regularly adopting a catalytic conformation, causing slower turnover (Table 1).

Benzoates with Strongly Electron-Withdrawing Substituents. The 3-NO_2- and 4-NO_2-BzO substrates were not productive, while 2-NO_2-BzO was turned over by BadA (Table 1). Similarly, 2-cyanobenzoate (2-CN-BzO) was the only productive substrate among the isomeric CN-BzO substrates but was ∼2.5-fold less active than 2-NO_2-BzO (Table 1). The K_M^{app} of BadA for 2-CN-BzO was ∼10-fold lower than for 2-NO_2-BzO (2000 μM). These data are consistent with the observation that substituent regiochemistry affects substrate binding and subsequent turnover.

Benzoates with Strongly Electron-Donating Substituents. The catalytic efficiency of 2-hydroxybenzoate (2-OH-BzO) was 16-fold lower than that of BzO, primarily because of its lower k_{cat}^{app} (Table 1). By comparison, the K_M^{app} values of BadA for 3-OH- and 4-OH-BzO were substantially higher than for 2-OH-BzO, yet 3-OH- and 4-OH-BzO were turned over similarly.

BadA did not bind 2-aminobenzoate (2-NH_2-BzO) (K_M^{app} = 21 μM) as well as 2-OH-BzO (1.6 μM) and was turned over 6-fold faster than 2-OH-Bz (Table 1). The catalytic efficiencies of BadA for 3-NH_2-BzO and 3-OH-BzO were similar (∼0.1 s^{-1} μM^{-1}) because of their comparable k_{cat}^{app} and K_M^{app} values. 4-NH_2-BzO binds BadA with ∼6-fold more apparent affinity (K_M^{app} = 25 μM) than the 4-OH-BzO (K_M^{app} = 160 μM), which is reciprocal to the ∼6-fold difference in product release (0.18 and 0.93 s^{-1}, respectively) of the corresponding CoA thioesters, thus equalizing the catalytic efficiencies of BadA for these substrates.

BadA turned over each Me-BzO regioisomer in almost the same order of reactivity as OH-, NH_2-, and Cl-substituted substrates (*ortho* > *meta* > *para*) (Table 1). The k_{cat}^{app} values for BadA with Me-BzO substrates compared with BzO were slower, and the K_M^{app} values were higher. The larger Michaelis constants were the dominant factors that affected the catalytic efficiency of BadA for the Me-substituted substrates. For the MeO-BzO substrates, BadA turned over 2-MeO-BzO 2000-fold slower than it did BzO, with a K_M^{app} 180-fold higher than that for BzO. 3-Methoxybenzoyl (3-MeO-Bz) CoA and 4-MeO-Bz CoA were not detectable under standard assay conditions and

DOI: 10.1021/acs.biochem.5b00899
Biochemistry 2015, 54, 6230−6242

Table 2. Relative Apparent Maximal Rates (V_{rel}^{app})[a] of BadA and Point Mutants for Various Substrates

		V_{rel}^{app}			
substituent on BzO	(V_{rel}^{app})[a] BadA	A227G	I334A	H333A	L332A
H (BzO)	100[b] (8.8)[c]	86 (4)	93 (3)	89 (10)	89 (8)
2-CH_3	10.6 (0.5)	42 (1)	1.8 (<0.1)	11 (1)	1.7 (0.2)
2-NO_2	1.6 (0.10)	1.2 (0.012)	0.03 (0.002)	1.4 (<0.1)	0.12 (0.01)
2-OCH_3	0.09 (0.008)	**10.4 (0.33)**	0.003 (<0.001)	0.058 (0.005)	0.004 (<0.001)
2-CN	0.02 (0.002)	**12.0 (0.82)**	0.03 (<0.01)	0.08 (0.01)	0.05 (0.002)
2,6-DiCl	ND[d]	**0.69 (0.02)**	ND[d]	ND[d]	ND[d]
3-CH_3	2.04 (0.4)	7.0 (0.3)	**49 (1.4)**	**44 (3.6)**	1.5 (0.12)
3-OCH_3	≤0.001	2.9 (0.32)	**70 (6.2)**	**10.7 (0.24)**	0.086 (0.009)
3-CN	ND[d]	0.038	**8.5 (1.3)**	**2.5 (0.15)**	0.017 (0.002)
3-NO_2	ND[d]	0.015 (0.0023)	0.23 (0.036)	**1.2 (0.034)**	ND[d]
4-CH_3	5.02 (0.304)	0.29 (0.014)	**14 (0.35)**	4.5 (0.202)	0.063 (0.004)
4-CN	≤0.001	≤0.001	0.010 (0.001)	**2.9 (0.3)**	ND[d]
4-OCH_3	ND[d]	<0.001	**39 (2.9)**	0.93 (0.019)	ND[d]
4-NO_2	ND[d]	ND[d]	≤0.001	**0.11 (0.010)**	ND[d]
4-ethyl	ND[d]	ND[d]	**9.4 (0.83)**	0.86 (0.058)	ND[d]
3,4-DiCH_3	<0.001	0.016 (0.0032)	ND[d]	0.69 (0.11)	ND[d]
(PhAc)	ND[d]	ND[d]	**0.012 (0.0022)**	<0.001	ND[d]

[a] V_{rel}^{app} values are normalized (as a percentage) to the apparent relative V_{max} of BadA for benzoate. Highlighted in bold are inactive substrates with BadA that are active with a mutant, or cases in which the mutant is 10-fold more active than BadA. [b] The V_{rel}^{app} for BadA with benzoate is 15.1 nmol/min. [c] Standard deviations are given in parentheses (n = 3). [d] Not detected.

were below the detection limit (at 0.5 pmol/mL) of the mass spectrometer.

Turnover of Heteroaromatic Carboxylates. BadA turned over the two heteroaromatics Thio-2-C and 3-Fur at similar rates (Table 1). The k_{cat}^{app} and the K_M^{app} of BadA for Thio-2-C are ∼6-fold slower and ∼8-fold higher, respectively, than the values for BzO, whereas the values for 3-Fur were ∼4-fold slower and ∼14-fold higher, respectively. These data showed that 3-Fur was turned over (1.4-fold) faster by BadA but had less apparent affinity (1.9-fold) for the enzyme than Thio-2-C, thus equalizing their catalytic efficiencies at ∼0.1 s^{-1} μM^{-1} (Table 1).

Turnover of Nonaromatic Carbocycle Carboxylates. Intrinsic k_{cat}^{app} values of BadA for nonaromatic carboxylates are reported here for the first time. The turnover rates of cyclohexane carboxylate, 1-cyclohexene-1-carboxylate (1-Cyc), and 3-cyclohexene-1-carboxylate (3-Cyc) were similar (only from 5- to 1.8-fold lower) to that of BzO. The K_M^{app} of cyclohexane carboxylate (Cyc) was ∼330-fold lower than that of BzO among these carbocycles. This trend is also reflected in the lower catalytic efficiency of BadA for Cyc than for 1-Cyc and 3-Cyc. However, the k_{cat}^{app} of BadA for Cyc was surprisingly 48% compared with the turnover of BzO. This result improves upon an earlier BadA study in which the relative apparent maximal rate (V_{rel}^{app}) was at 1% for Cyc compared with that for BzO, likely because of a low Cyc concentration (250 μM),[12] below the calculated K_M^{app} of 1470 μM in this study.

Rational Mutation of the BadA Active Site. BadA structures in complex with carboxylate substrates and a benzoyl-AMP intermediate guided site-directed mutagenesis on the wild-type BadA to remove steric bulk from the active site and expand the substrate preference for benzoates with *meta* and *para* substituents. Four residues (Ala227, Leu332, His333, and Ile334) surround the phenyl ring of BzO in the active site (Figure 5). The residue positioned near a given carbon of BzO depends on whether the BzO is in the carboxylate-bound orientation (Figure 5A) or the rotated Bz-AMP-bound orientation (Figure 5B). For example, Ala227 is next to the *meta* carbon of BzO (Figure 5A) and the *ortho* carbon of Bz-AMP (Figure 5B). Similarly, the peptide backbone of Leu332 is near the *para* and *meta* carbons of BzO and Bz-AMP, respectively. The His333 side chain points toward the *meta* and *para* positions of BzO and Bz-AMP, respectively, while the Ile334 side chain is near the *ortho* carbon of BzO and the *meta* carbon of Bz-AMP. Therefore, targeted mutations of Ala227Gly, Leu332Ala, His333Ala, and Ile334Ala should show the relative importance of the two orientations for reactivity. The latter three were mutated to Ala instead of a smaller, flexible Gly to maintain conformational rigidity in the peptide backbone. Each mutant turned over the natural substrate benzoate at 86−93% of the rate of BadA (Table 2).

Ala227Gly-BadA Mutant. The maximal relative velocities (V_{rel}^{app}) of the Ala227Gly-BadA mutant increased for *ortho*-substituted BzO substrates [2-Me (∼4-fold), 2-CN (600-fold), and 2-MeO (116-fold)] compared with those of BadA. Ala227Gly-BadA also uniquely converted 2,6-dichlorobenzoate (2,6-diCl-BzO) to its CoA thioester, while BadA and the other mutant enzymes did not. Increases in activity with *meta*-substituted BzO substrates were also observed. An ∼3-fold increase in activity with 3-Me-BzO was observed in addition to an ∼2900-fold (or greater) increase in activity with 3-MeO-BzO. Novel but low-level activities with 3-CN-BzO and 3-NO_2-BzO were observed. Compared with the activities of BadA for substrates with *para* substituents, the mutant activities were roughly the same, except the mutation markedly decreased the rate of turnover of 4-Me-BzO by 17-fold (Table 2).

Ile334Ala-BadA Mutant. The Ile334Ala-BadA mutant had higher V_{rel}^{app} values for *meta*- and *para*-substituted benzoates but lower values for all *ortho*-substituted benzoates tested. The V_{rel}^{app} values of Ile334Ala-BadA compared with those of BadA increased 70000-fold for 3-MeO-BzO, 24-fold for 3-Me-BzO, 2.8-fold for 4-Me-BzO, and 7-fold for 4-CN-BzO (Table 2). The Ile334Ala-BadA mutant had expanded substrate specificity for previously inactive substrates: 4-MeO (39%), 4-ethyl-benzoate (4-ethyl-BzO) (9.4%), 3-CN-BzO (8.5%), 3-NO_2-BzO (0.2%), a benzoate homologue, phenylacetate (PhAc)

DOI: 10.1021/acs.biochem.5b00899
Biochemistry 2015, 54, 6230−6242

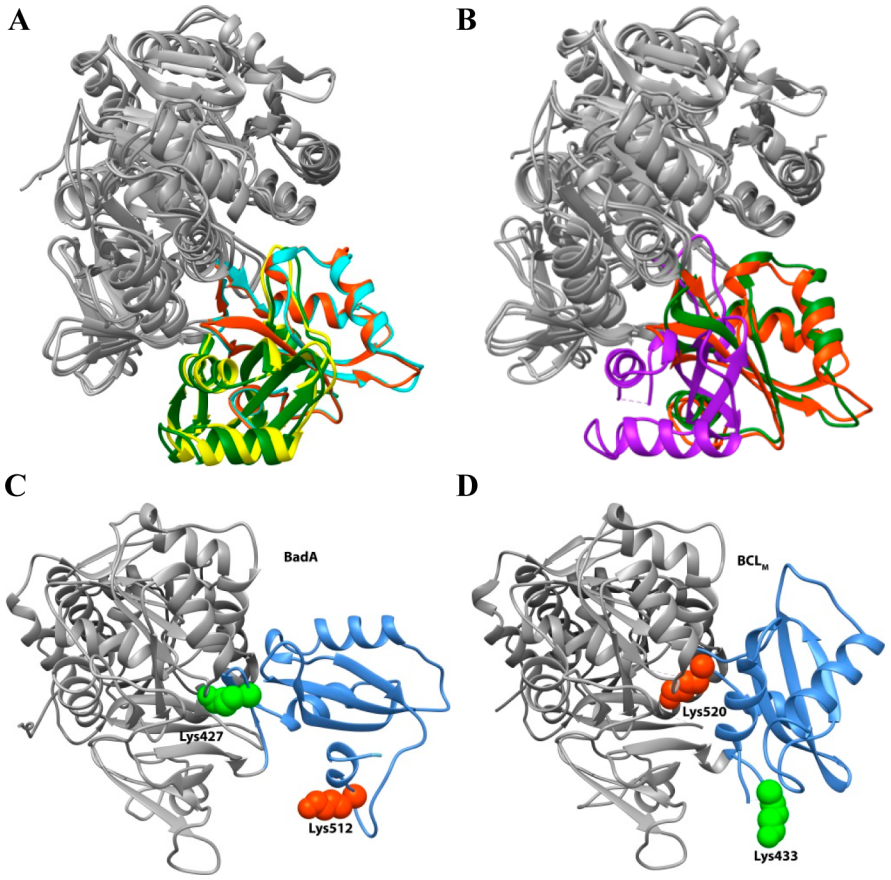

Figure 6. (A) C-Terminal domains (ligands are omitted for clarity) of CBAL in complex with 4-Cl-BzO (PDB entry 1T5D) (green) and 4-Cl-Bz-AMP (PDB entry 3CW8) (yellow), in the adenylation conformation, are overlaid with those of BadA in complex with BzO (PDB entry 4EAT) (red) and Bz-AMP (PDB entry 4ZJZ) (cyan) in the thiolation conformation. (B) C-Terminal domains (ligands omitted for the sake of clarity) of CBAL in complex with both 4-chlorophenacyl CoA and AMP (PDB entry 3CW9) (green) and BCL_M in complex with BzO (PDB entry 2V7B) (purple) are overlaid with that of BadA in complex with BzO (PDB entry 4EAT) (red) in the thiolation conformation. (C) Relative positions of catalytically important lysine residues in BadA and BCL_M. The C-terminal domain (blue) is in the thiolation conformation: Lys427 (green) of BadA (PDB entry 4ZJZ) is in the active site, and Lys512 (red) is solvent-exposed. (D) The C-terminal domain (blue) is in the adenylation conformation: Lys520 (red) of BCL_M (PDB entry 2V7B) is in the active site, and Lys433 (green) is solvent-exposed. N-Terminal domains are colored gray.

(0.01%), and 4-NO_2-BzO (0.001%) (Table 2). The Ile334Ala mutation, designed to help binding and turnover of BadA for *ortho*-substituted substrates, dramatically increased the rate of catalysis of larger *meta* and *para* substituents.

His333Ala-BadA Mutant. His333Ala-BadA mutant, designed to help binding and turnover of BzO substrates with substituents at the *meta* position, resulted in increases in activity with both *meta*- and *para*-substituted BzO substrates but did not significantly change the V_{rel}^{app} for *ortho*-substituted BzO substrates compared to that of BadA. Compared with that of BadA, the V_{rel}^{app} values of His333Ala-BadA increased 11000-fold for 3-MeO-BzO, 22-fold for 3-Me-BzO, 3400-fold for 3,4-diMe-BzO, and 2100-fold for 4-CN-BzO (Table 2). New activities [relative to BzO (at 100%)] for this mutation include 3-CN-BzO (2.5%), 3-NO_2-BzO (1.2%), 4-MeO-BzO (0.9%), 4-NO_2-BzO (0.1%), and 4-ethyl-BzO (0.9%) substrates (Table 2).

Leu332Ala-BadA Mutant. The Leu332Ala mutant was designed to increase the rate of binding and turnover of *para*-substituted benzoic acids. Upon testing this mutant, we observed a significant loss of activity (~90%) for nearly all substrates except BzO. Small increases in activity with 3-MeO-BzO and 3-CN-BzO were observed. The Leu332Ala mutant turned over BzO at 89% of the rate of BadA; other mutants tested turned over the natural substrate at a similar rate.

DISCUSSION

In this study, to provide insight into active site residues that define substrate selectivity, we determined the crystal structure of BadA and used this information to design point mutants with greater substrate permissivity. In addition, we measured the Michaelis parameters of BadA for various substrates to evaluate how steric effects and electronics, through interactions with a heteroatom or substituent, affect binding and turnover.

BadA Structure and Homology. Homologous adenylase structures of CoA ligases and AMP ligases (20−30% similar) in the PDB (including BadA) show that enzymes in this family typically fold into a larger N-terminal domain (400−550 residues) and a smaller C-terminal domain (~110 residues), where the active site lies between the domains. The N-terminal domain contains nearly all the residues that bind the carboxylate substrate. The N-terminal domain also binds the adenosyl group of ATP, while the C-terminal domain residues coordinate the ribose and phosphate groups. Several related CoA ligase crystal structures support a domain alternation mechanism in which the C-terminal domain rotates ~140° from its adenylation conformation to a thiolation conformation after the acyl-AMP forms and CoA binds.[21] The domain rotation occurs on a flexible hinge loop that contains a conserved Asp residue,[26] and this conformational change

DOI: 10.1021/acs.biochem.5b00899
Biochemistry 2015, 54, 6230−6242

configures the ligase for the thiolation step in the second half-reaction.[44] The adenylation conformation supposedly forms when the carboxylate alone (or with ATP) binds the active site in the N-terminal domain.[24,26] After the formation of the acyl anhydride intermediate and binding of CoA, the C-terminal domain rotates into the thiolation conformation. This rotation places key catalytic C-terminal residues in the active site and primes the enzyme for thioesterification.[21,26,45]

To the best of our knowledge, all known structures of ATP-dependent aroyl CoA ligases in complex with only their natural carboxylate substrate adopt the adenylation conformation.[14,23,25,28] The structure of a 4-chlorobenzoate CoA ligase (CBAL) from *Alcaligenes* sp. AL3007 in complex with 4-chlorobenzoate (4-Cl-BzO) (PDB entry 1T5D) or 4-Cl-Bz-AMP (PDB entry 3CW8) adopts the adenylation conformation (Figure 6A). Subsequently, CBAL adopts the CoA-bound thiolation conformation when complexed with a phenacyl analogue of 4-chlorobenzoyl CoA and AMP (PDB entry 3CW9) (Figure 6B). The crystal structure of a benzoate CoA ligase (BCL_M) (PDB entry 2V7B) from *B. xenoverans*[14] (61% sequence identity with BadA), in complex with only benzoate, is in the adenylation conformation (Figure 6B). In contrast, all six BadA structures in complex with either aryl carboxylates or Bz-AMP are found surprisingly in the thiolation conformation, even in the absence of CoA. This observation deviates from the predicted sequential domain alternation mechanism proposed for ATP-dependent CoA ligases.[21] The conserved Asp424 hinge residue in BadA and the flanking residues of the flexible loop are nearly identical with those in BCL_M. Reasons for why the BadA and BCL_M structures adopt different C-domain conformations when bound to aryl carboxylate substrates remain obscure, particularly because a BadA structure in the adenylation conformation is unavailable. However, one possible explanation is that the two enzymes have different resting states; BadA assumes the thiolation conformation, while BCL_M adopts the adenylation conformation when benzoate is bound.

Further, sequence and structural alignments show that the active site residues (Figure S28 of the Supporting Information) and architectures of the N-terminal domains of BadA and BCL_M in complex with benzoate are identical. It is therefore interesting that the relative k_{cat}^{app} values for BadA with fluorobenzoates ranged between 75 and 117% relative to that of BzO (100%), whereas BCL_M turned over 2-F-BzO at 2% of the rate for BzO.[14] Active site residue Phe236 in the adenylation conformation of BCL_M is located <4 Å above the carboxylate group of the bound BzO and blocks the CoA channel. The analogous Phe226 residue in BadA is offset by an ~72° rotation away from the BzO, opening the CoA binding channel (Figure S29 of the Supporting Information). Because the BadA and BCL_M structures have different C-domain conformations, it is difficult to provide a structural rationale for differences in substrate specificity between BadA and BCL_M.

Catalytically Important Lysine Residues in BadA. Despite the different conformations of the C-terminal domain for BadA and BCL_M, each uses a distinct C-terminal domain lysine (Lys427/512 for BadA and Lys433/520 for BCL_M) to orient the BzO substrate in either conformational state. In the adenylation conformation, BCL_M uses Lys520 (aligns with Lys512 of BadA) to coordinate BzO. An earlier study showed that mutation to alanine or modification by native enzymatic N^{ϵ}-acetylation of Lys512 of BadA reduced the extent of benzoyl CoA product formation by 99%.[30,46] In all BadA structures in the thiolation conformation presented here, Lys427 coordinates BzO in the active site and Lys512 is far from the active site and solvent-exposed in the C-domain (Figure 6C,D). The apo structure of ACSM2A crystallized in the thiolation conformation, supporting the idea that this conformation is available for binding by the carboxylate ligand.[24] A thiolation conformation resting state would make the conserved lysine (Lys512 of BadA), present in all ATP-dependent CoA ligases, solvent accessible for post-translational regulation by N^{ϵ}-acetyltransferases/deacetylases.[30,46,47]

The surface-exposed, conserved lysine residue is accessible to regulatory acetyltransferases/deacetylases when these ligases adopt the thiolation conformation. By contrast, the adenylation conformation returns this lysine to the active site for adenylation catalysis. Lys427 of BadA makes four polar contacts with Bz-AMP, one with the benzoyl oxygen, three with the AMP moiety, and two to Gly303 and Gly430 (Figure 7). These

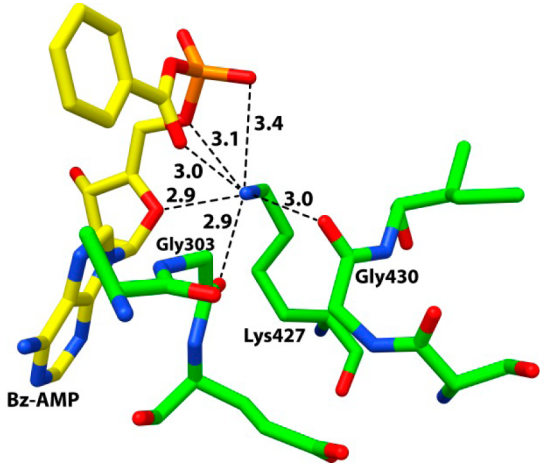

Figure 7. Active site of BadA showing possible polar contacts between Lys427 and Bz-AMP ligand (yellow), Gly304, and Gly431 (green). Distances (in angstroms) are shown. Heteroatoms are colored as red for oxygen, orange for phosphorus, and blue for nitrogen.

contacts likely anchor Bz-AMP, and the positive charge of Lys427 primes the AMP leaving group for CoA transesterification. On the basis of this information, we predicted a Lys427Ala-BadA mutant would slow the second thioesterification step of the BadA reaction and found indeed that the mutant was 99.9% less active than BadA. However, the rate of acyl-AMP formation appears to be unaffected. In the absence of structural data, the importance of Lys427 of BadA on catalysis was unexpected because of the semiconserved nature of the residue.

Together, the earlier Lys512 modification study and the Lys427 mutagenesis described here suggest that when BadA assumes the adenylation conformation (likely stabilized when ATP binds), Lys512 enters the active site. It is imagined that the latter residue then coordinates and primes BzO for nucleophilic attack on ATP based on homology with BCL_M in the adenylation conformation. This mechanistic sequence is analogous to that described in an earlier study for ACSM2A.[24] The latter proceeds through a proposed series of conformations [thiolation (carboxylate binding step), adenylation (ATP binding step), and returns to thiolation (acyl-AMP forming, CoA binding, and thioesterification steps)] to catalyze its thioesterification reaction.

Lys427 is not highly conserved among ligases; however, BCL_M contains a presumed functionally similar lysine residue

DOI: 10.1021/acs.biochem.5b00899
Biochemistry 2015, 54, 6230−6242

(Lys433) at the same position as the active site Lys427 of BadA, as does the phenylalanine adenylation domain (PheA) of gramicidin synthetase I from *Brevibacillus brevis*, and the D-alanyl carrier protein ligase (DltA) from *Bacillus cereus*.[28,48] In other ligases, such as the dihydroxybenzoate CoA ligase (DhbE) from *Bacillus subtilis* (Asn434) or 4-chlorobenzoate CoA ligase (CBAL) (Ile406), other residues[23,25] align with Lys427 of BadA (see Figure S30 of the Supporting Information). These residues are predicted to be oriented like Lys427 of BadA in the thiolation conformation based upon sequence and structural alignments. The importance of Lys427 for BadA catalysis of the thioesterification reaction led us to postulate that lysine surrogates of DhbE and CBAL perform a similar function in stabilizing the acyl-AMP intermediate. Likely, a combination of Asn434 and Arg428 of DhbE and Asn411 and Arg400 of CBAL (similar to the highly conserved Arg421 of BadA) forms polar contacts with the acyl-AMP intermediates. We anticipate that lysine residues or nearby polar residues positioned like Lys427 and Arg421 of BadA are important for thioesterification in other ATP-dependent CoA ligases.

Structural Rationale for Substrate Specificity of BadA. Through structural characterization of BadA, the different trajectories of BzO and the pathway intermediate Bz-AMP suggest that the substrate must rotate ∼60° counterclockwise [relative to the *re*-face (see Figure 5D)] about the C_6 axis. This rotation causes the ring carbons of BzO to move past multiple active site residues to access the Bz-AMP trajectory (Figure 5D). Upon binding BzO, the residues in BadA closest (≤3.8 Å) to one *ortho* carbon are Ile334 and Ala302. The other *ortho* carbon points toward a void within the active site where the phosphate group of Bz-AMP will ultimately reside (Figure 5 and Figure S31), supporting the favored binding of *ortho*-substituted benzoates in BadA. The structures of *ortho*-substituted benzoates bound to BadA all show them oriented such that the substituents occupy this void region and are not pointed toward Ile334 and Ala302. The *meta* carbons of the benzoates align with Ala227 and His333, and the *para* carbon is nearest the carbonyl of Leu332 on the peptide backbone. The effects of the steric residues were evidenced generally by the higher K_M^{app} values of BadA for *meta* and *para* substituents with increasing covalent van der Waals volumes F < OH < NH_2 < CN < Cl < Me < NO_2 < MeO of benzoates (Table S2) over the *ortho* regioisomers (Table 1).

When the substrate rotates toward the Bz-AMP conformation, the steric active site residues presumably reduced access to the catalytically proper orientation and generally also slowed the k_{cat}^{app} of BadA for substrates with larger substituents (Table 1). BadA typically turned over 2-substituted substrates faster than the 3- and 4-substituted isomers. The observation is consistent with the kinetic data for substrates other than the F-BzO series. Fluorine is a bioisostere of hydrogen,[43,49] and thus, the steric demand of the F-BzO substrates is similar to that of BzO, as reflected in the similar K_M^{app} values of BadA for 2- and 4-F-BzO and BzO. However, overall, the enzyme turnover and binding affinity are principally affected by the regiochemistry and steric effects of the substituents (Table 1). For instance, BadA turned over 2-MeO-BzO presumably only by placing the bulky methoxy group toward the open channel in the active site. We imagine the bulky methoxy group clashed with Ala227 before and after rotation of the benzoyl moiety of the substrate. As a result, the binding affinity and turnover of BadA were reduced for 2-MeO-BzO compared to those of BzO, and 3- and 4-MeO-BzO were not productive.

Attempts to cocrystallize BadA with 4-Me-BzO (98% purity) intriguingly resulted in a structure containing the 2-methyl isomer (not shown). This isomeric selection strongly supported the idea that weakened steric interactions in the active site around one *ortho* carbon of the substrate allowed highly regiospecific binding of *ortho*-substituted substrates. It is worth noting that 2-OH-BzO had the lowest K_M^{app} of all substrates tested with BadA. Evaluation of the BadA−BzO complex suggests that the 2-OH group may interact with the nearby hydroxyl of Thr329, creating a second binding contact (Figure 5D). In addition to interacting with the carboxylate of the bound BzO, Thr329, creating a second binding contact (Figure 5D) that may also affect the release of the 2-OH-Bz CoA as shown by the faster release of the 3- and 4-OH-Bz CoA products.

Similarly, the regiochemistries of the splayed, planar NO_2 group and the extended, linear CN substituent likely prevented 3-NO_2-, 3-CN-, 4-NO_2-, and 4-CN-BzO from binding and being turned over by BadA. As with the bulky 2-MeO-BzO substrate, 2-NO_2- and 2-CN-BzO were productive and converted slowly to their CoA thioesters by BadA (Table 1). The linear 2-CN substituent extends into the open channel of the active site (Figure 5A,D).[43] The k_{cat}^{app} for 2-CN-BzO, however, is lower than nearly all of the values of the 2-substituted BzO substrates with smaller substituents, and this observation is consistent with the steric effects of Ala227 affecting catalysis as the substrate pivots during adenylation. To illustrate further, *ortho*-substituted substrates 2-CN-BzO (K_M^{app} = 213 μM) and 2-Cl-BzO (K_M^{app} = 130 μM) bind BadA similarly. However, the estimated covalent van der Waals length of cyano (C_{Ar}−CN; d_w = 3.1 Å) extends further than that of chloro (C_{Ar}−Cl; d_w = 2.5 Å) (ChemBioDraw, version 13.0), and this difference may have reduced the k_{cat}^{app} of BadA for 2-CN-BzO by 200-fold compared with that for 2-Cl-BzO.

In summary, the size and position of the substituent on a BzO analogue affect the relative rates of reactivity significantly more than the electronics of the substituent. BadA is more forgiving of *ortho* substituents than *para* substituents, consistent with the relatively open channel in the BadA structures next to the *ortho* carbon of the BzO substrate. In contrast, substituents at the *meta* and *para* positions significantly impact activity, except for fluorinated substituents, which are isosteric with hydrogen and thus have no additional steric requirements.

Nonaromatic Carbocycle Carboxylates. The Cyc substrate bound BadA the worst among the nonaromatic carbocycles likely because the staggered ring conformations and additional hydrogens clashed with active site residues. Estimated by K_M^{app}, substrates 1-Cyc and 3-Cyc have ∼12−13-fold more apparent affinity for BadA than cyclohexane (Table 1). The planarity of the double bond in these mono-unsaturated carbocycles likely reduced steric interfaces between the ring and active site residues within the BadA active site. The rate of turnover of 1-Cyc was lower than that for Cyc (Table 1), while the placement of the double bond in 3-Cyc strongly increased the rate of catalytic turnover. The double bond positioned between the *meta* and *para* carbons of the ring in the latter removes two hydrogen atoms from the substrate that binds in a sterically crowded area near Ala227. Decreasing this steric hindrance likely explains the higher rate of turnover and lower K_M^{app} of 3-Cyc relative to those of Cyc and 1-Cyc (Table 1).

DOI: 10.1021/acs.biochem.5b00899
Biochemistry 2015, 54, 6230−6242

Analysis of Point Mutants of BadA. Mutational analyses also supported the substrate rotation mechanism in the BadA active site during catalysis. The four mutants Ala227Gly-BadA, Ile334Ala-BadA, His333Ala-BadA, and Leu332Ala-BadA in this study were designed to reduce the steric clash encountered by the substituents during substrate binding and rotation to form Bz-AMP within BadA. For example, the proposed 60° rotation causes the *ortho* and *meta* carbons of the initially bound BzO to move to the former locations of the *meta* and *para* carbons, respectively. Support for substrate rotation arises from a representative Ala227Gly-BadA mutation that weakened the steric interactions near the *ortho* and *meta* carbons of BzO. This mutant showed increased activity over BadA for *ortho*-substituted substrates that were imagined to bind and rotate within a sterically more favorable active site. This same mutant showed low but novel activities with *meta*-substituted BzO substrates, suggesting that the Ala227Gly mutation allowed *meta*-substituted substrates to now bind and rotate to a catalytically competent adenylation orientation (Table 2).

Collectively, the Ala227Gly-BadA, Ile334Ala-BadA, and His333Ala-BadA mutants turned over new substrates [3-MeO, 3-CN, 3-NO_2, 4-MeO, 4-NO_2, 4-ethyl, 3,4-Di-CH_3, and, surprisingly, phenylacetate (PhAc), a precursor of penicillin G] that BadA could not (Table 2). Ile334Ala-BadA and His333Ala-BadA were active with nearly all of the 16 substrates tested, including PhAc, making these mutants broadly active 2-, 3-, or 4-substituted benzoate CoA ligases. Ala227Gly-BadA uniquely turned over 2,6-DiCl-BzO. The results of the point mutations of BadA again supported a steric argument for BadA reactivity as opposed to one for substituent electronic effects. It is unclear why the Leu332Ala-BadA mutant, designed to weaken the steric interactions around the *para* carbon of the substrate, unexpectedly did not turn over the *para*-substituted analogues and slowed the turnover of several non-natural substrates tested (Table 2). The peptide backbone carbonyl of Leu332 contributes to the active site architecture, while the Leu side chain is oriented away from the active site. The Leu side chain most likely engages in structural, hydrophobic interactions (see Figure 5A,B). Therefore, we suspect the Leu332Ala mutation may have malformed the active site of BadA.

CONCLUSION

Structures of BadA in complex with aryl carboxylate or aryl carbonyl-AMP show a persistent thiolation conformation before adenylation or CoA binding. This pre-CoA-bound conformation of BadA deviates from available structures of bacterial aryl carboxylate CoA ligases in the PDB. This suggests that the enzyme dynamics of BadA may be unique among benzoate CoA ligases during the substrate binding, adenylation, and CoA thioesterification steps. Thus, we propose two possible subclasses of benzoate CoA ligases, (i) those whose thiolation conformation is the resting state and therefore bind benzoate in this conformation and (ii) those whose resting state is the adenylation conformation and bind benzoate in this conformation. Additional biochemical and structural analyses are required to further support this hypothesis. Further, similarity in the protein architecture and ligands bound, yet differences in the overall tertiary protein structure, aid in understanding the mechanisms of action. With this understanding, it was possible to design mutant constructs that were dramatically more permissive than the native protein. The Ala227Gly-BadA mutant improved catalysis primarily with *ortho*-substituted benzoates, while Ile334Ala-BadA and His333Ala-BadA improved turnover with *meta*- and *para*-substituted benzoates over native BadA catalysis. These findings are important for making non-natural acyl CoA thioesters that can be used in a chassis organism engineered to express natural product pathways that make next-generation bioactive compounds. Expanding the BadA substrate specificity may also help in engineering pathways for bioremediation where substrate specificity is often a bottleneck for strain development[50] against pollutants like polycyclic aromatic hydrocarbons[51] and polychlorinated biphenyls.[52,53] In addition, the BadA kinetic constants provide data needed for modeling flux control analysis in synthetic biology and bioengineering,[54−57] as well as metabolizing carboxylate-containing xenobiotic drugs in animals.[24]

ASSOCIATED CONTENT

Supporting Information

The Supporting Information is available free of charge on the ACS Publications website at DOI: 10.1021/acs.biochem.5b00899.

Chemicals, plasmids, Michaelis−Menten plots for the ligase reaction, and additional protein structure figures and sequence alignments (PDF)

AUTHOR INFORMATION

Corresponding Authors

*E-mail: walker@chemistry.msu.edu.
*E-mail: geiger@chemistry.msu.edu.

Funding

Michigan State University AgBioResearch Grant RA078692 (894) (to K.D.W.) and U.S. Department of Energy Contract DE-FG02-06ER15822 (to J.H.G.).

Notes

The authors declare no competing financial interest.

ACKNOWLEDGMENTS

We thank Caroline Harwood (University of Washington, Seattle, WA) for the *badA* gene. We thank the Michigan State University Research Technology Support Facility: Mass Spectrometry and Metabolomics Core for their technical assistance. This research used resources of the Advanced Photon Source, a U.S. Department of Energy (DOE) Office of Science User Facility operated for the DOE Office of Science by Argonne National Laboratory under Contract DE-AC02-06CH11357. Use of the LS-CAT Sector 21 was supported by the Michigan Economic Development Corp. and the Michigan Technology Tri-Corridor (Grant 085P1000817). Molecular graphics were created and analyses performed with the UCSF Chimera package. Chimera is developed by the Resource for Biocomputing, Visualization, and Informatics at the University of California, San Francisco (supported by National Institute of General Medical Sciences Grant P41-GM103311).

ABBREVIATIONS

BzO, benzoate; CoA, coenzyme A; AMP, adenosine monophosphate; HPLC, high-performance liquid chromatography; MS, mass spectrometry.

DOI: 10.1021/acs.biochem.5b00899
Biochemistry 2015, 54, 6230−6242

REFERENCES

(1) Schmelz, S., and Naismith, J. H. (2009) Adenylate-forming enzymes. *Curr. Opin. Struct. Biol. 19*, 666−671.

(2) Conti, E., Franks, N. P., and Brick, P. (1996) Crystal structure of firefly luciferase throws light on a superfamily of adenylate-forming enzymes. *Structure 4*, 287−298.

(3) Schmelz, S., Kadi, N., McMahon, S. A., Song, L., Oves-Costales, D., Oke, M., Liu, H., Johnson, K. A., Carter, L. G., Botting, C. H., White, M. F., Challis, G. L., and Naismith, J. H. (2009) AcsD catalyzes enantioselective citrate desymmetrization in siderophore biosynthesis. *Nat. Chem. Biol. 5*, 174−182.

(4) Storz, M. P., Brengel, C., Weidel, E., Hoffmann, M., Hollemeyer, K., Steinbach, A., Muller, R., Empting, M., and Hartmann, R. W. (2013) Biochemical and biophysical analysis of a chiral PqsD inhibitor revealing tight-binding behavior and enantiomers with contrary thermodynamic signatures. *ACS Chem. Biol. 8*, 2794−2801.

(5) Bonet, B., Teufel, R., Crüsemann, M., Ziemert, N., and Moore, B. S. (2015) Direct capture and heterologous expression of *Salinispora* natural product genes for the biosynthesis of enterocin. *J. Nat. Prod. 78*, 539−542.

(6) Walker, K., Long, R., and Croteau, R. (2002) The final acylation step in Taxol biosynthesis: Cloning of the taxoid C13-side-chain *N*-benzoyltransferase from *Taxus*. *Proc. Natl. Acad. Sci. U. S. A. 99*, 9166−9171.

(7) Walker, K., and Croteau, R. (2000) Taxol biosynthesis: Molecular cloning of a benzoyl-CoA: taxane 2α-O-benzoyltransferase cDNA from *Taxus* and functional expression in *Escherichia coli*. *Proc. Natl. Acad. Sci. U. S. A. 97*, 13591−13596.

(8) Dudareva, N., Klempien, A., Muhlemann, J. K., and Kaplan, I. (2013) Biosynthesis, function and metabolic engineering of plant volatile organic compounds. *New Phytol. 198*, 16−32.

(9) Ziehl, M., He, J., Dahse, H.-M., and Hertweck, C. (2005) Mutasynthesis of aureonitrile: An aureothin derivative with significantly improved cytostatic effect. *Angew. Chem., Int. Ed. 44*, 1202−1205.

(10) He, J., and Hertweck, C. (2003) Iteration as programmed event during polyketide assembly; molecular analysis of the aureothin biosynthesis gene cluster. *Chem. Biol. 10*, 1225−1232.

(11) Coleman, J. P., Hudson, L. L., McKnight, S. L., Farrow, J. M., III, Calfee, M. W., Lindsey, C. A., and Pesci, E. C. (2008) *Pseudomonas aeruginosa* PqsA is an anthranilate-coenzyme A ligase. *J. Bacteriol. 190*, 1247−1255.

(12) Geissler, J. F., Harwood, C. S., and Gibson, J. (1988) Purification and properties of benzoate-coenzyme A ligase, a *Rhodopseudomonas palustris* enzyme involved in the anaerobic degradation of benzoate. *J. Bacteriol. 170*, 1709−1714.

(13) Egland, P. G., Gibson, J., and Harwood, C. S. (1995) Benzoate-coenzyme a ligase, encoded by BadA, is one of 3 ligases able to catalyze benzoyl-coenzyme A formation during anaerobic growth of *Rhodopseudomonas palustris* on benzoate. *J. Bacteriol. 177*, 6545−6551.

(14) Bains, J., and Boulanger, M. J. (2007) Biochemical and structural characterization of the paralogous benzoate CoA ligases from *Burkholderia xenovorans* LB400: Defining the entry point into the novel benzoate oxidation (box) pathway. *J. Mol. Biol. 373*, 965−977.

(15) Chang, K. H., Xiang, H., and Dunaway-Mariano, D. (1997) Acyl-adenylate motif of the acyl-adenylate/thioester-forming enzyme superfamily: A site-directed mutagenesis study with the *Pseudomonas* sp. strain CBS3 4-chlorobenzoate:coenzyme A ligase. *Biochemistry 36*, 15650−15659.

(16) Schuhle, K., Gescher, J., Feil, U., Paul, M., Jahn, M., Schagger, H., and Fuchs, G. (2003) Benzoate-coenzyme A ligase from *Thauera aromatica*: An enzyme acting in anaerobic and aerobic pathways. *J. Bacteriol. 185*, 4920−4929.

(17) Carmona, M., Zamarro, M. T., Blazquez, B., Durante-Rodriguez, G., Juarez, J. F., Valderrama, J. A., Barragan, M. J., Garcia, J. L., and Diaz, E. (2009) Anaerobic catabolism of aromatic compounds: A genetic and genomic view. *Microbiol. Mol. Biol. Rev. 73*, 71−133.

(18) Fuchs, G. (2008) Anaerobic metabolism of aromatic compounds. *Ann. N. Y. Acad. Sci. 1125*, 82−99.

(19) Seo, J. S., Keum, Y. S., and Li, Q. X. (2009) Bacterial degradation of aromatic compounds. *Int. J. Environ. Res. Public Health 6*, 278−309.

(20) Berg, P. (1956) Acyl adenylates: An enzymatic mechanism of acetate activation. *J. Biol. Chem. 222*, 991−1013.

(21) Reger, A. S., Wu, R., Dunaway-Mariano, D., and Gulick, A. M. (2008) Structural characterization of a 140° domain movement in the two-step reaction catalyzed by 4-chlorobenzoate:CoA ligase. *Biochemistry 47*, 8016−8025.

(22) Muchiri, R., and Walker, K. D. (2012) Taxol biosynthesis: Tyrocidine synthetase A catalyzes the production of phenylisoserinyl CoA and other amino phenylpropanoyl thioesters. *Chem. Biol. 19*, 679−685.

(23) May, J. J., Kessler, N., Marahiel, M. A., and Stubbs, M. T. (2002) Crystal structure of DhbE, an archetype for aryl acid activating domains of modular nonribosomal peptide synthetases. *Proc. Natl. Acad. Sci. U. S. A. 99*, 12120−12125.

(24) Kochan, G., Pilka, E. S., von Delft, F., Oppermann, U., and Yue, W. W. (2009) Structural snapshots for the conformation-dependent catalysis by human medium-chain acyl-coenzyme A synthetase ACSM2A. *J. Mol. Biol. 388*, 997−1008.

(25) Gulick, A. M., Lu, X., and Dunaway-Mariano, D. (2004) Crystal structure of 4-chlorobenzoate:CoA ligase/synthetase in the unliganded and aryl substrate-bound states. *Biochemistry 43*, 8670−8679.

(26) Reger, A. S., Carney, J. M., and Gulick, A. M. (2007) Biochemical and crystallographic analysis of substrate binding and conformational changes in acetyl-CoA synthetase. *Biochemistry 46*, 6536−6546.

(27) Hu, Y., Gai, Y., Yin, L., Wang, X., Feng, C., Feng, L., Li, D., Jiang, X. N., and Wang, D. C. (2010) Crystal structures of a *Populus tomentosa* 4-coumarate:CoA ligase shed light on its enzymatic mechanisms. *Plant Cell 22*, 3093−3104.

(28) Conti, E., Stachelhaus, T., Marahiel, M. A., and Brick, P. (1997) Structural basis for the activation of phenylalanine in the non-ribosomal biosynthesis of gramicidin S. *EMBO J. 16*, 4174−4183.

(29) Berg, P. (1956) Acyl adenylates: The synthesis and properties of adenyl acetate. *J. Biol. Chem. 222*, 1015−1023.

(30) Crosby, H. A., Heiniger, E. K., Harwood, C. S., and Escalante-Semerena, J. C. (2010) Reversible N^{ε}-lysine acetylation regulates the activity of acyl-CoA synthetases involved in anaerobic benzoate catabolism in *Rhodopseudomonas palustris*. *Mol. Microbiol. 76*, 874−888.

(31) Beuerle, T., and Pichersky, E. (2002) Purification and characterization of benzoate:coenzyme A ligase from *Clarkia breweri*. *Arch. Biochem. Biophys. 400*, 258−264.

(32) Gaid, M. M., Scharnhop, H., Ramadan, H., Beuerle, T., and Beerhues, L. (2011) 4-Coumarate:CoA ligase family members from elicitor-treated *Sorbus aucuparia* cell cultures. *J. Plant Physiol. 168*, 944−951.

(33) Otwinowski, Z., and Minor, W. (1997) Processing of X-ray diffraction data collected in oscillation mode. *Methods Enzymol. 276*, 307−326.

(34) Arnold, K., Bordoli, L., Kopp, J., and Schwede, T. (2006) The SWISS-MODEL workspace: A web-based environment for protein structure homology modelling. *Bioinformatics 22*, 195−201.

(35) Winn, M. D., Ballard, C. C., Cowtan, K. D., Dodson, E. J., Emsley, P., Evans, P. R., Keegan, R. M., Krissinel, E. B., Leslie, A. G. W., McCoy, A., McNicholas, S. J., Murshudov, G. N., Pannu, N. S., Potterton, E. A., Powell, H. R., Read, R. J., Vagin, A., and Wilson, K. S. (2011) Overview of the CCP4 suite and current developments. *Acta Crystallogr., Sect. D: Biol. Crystallogr. 67*, 235−242.

(36) Vagin, A., and Teplyakov, A. (1997) MOLREP: An automated program for molecular replacement. *J. Appl. Crystallogr. 30*, 1022−1025.

(37) Vagin, A. A., Steiner, R. A., Lebedev, A. A., Potterton, L., McNicholas, S., Long, F., and Murshudov, G. N. (2004) REFMAC5 dictionary: Organization of prior chemical knowledge and guidelines for its use. *Acta Crystallogr., Sect. D: Biol. Crystallogr. 60*, 2184−2195.

DOI: 10.1021/acs.biochem.5b00899
Biochemistry 2015, 54, 6230−6242

(38) Emsley, P., Lohkamp, B., Scott, W. G., and Cowtan, K. (2010) Features and development of COOT. *Acta Crystallogr., Sect. D: Biol. Crystallogr. 66*, 486−501.
(39) Lebedev, A. A., Young, P., Isupov, M. N., Moroz, O. V., Vagin, A. A., and Murshudov, G. N. (2012) JLigand: A graphical tool for the CCP4 template-restraint library. *Acta Crystallogr., Sect. D: Biol. Crystallogr. 68*, 431−440.
(40) Connolly, M. L. (1993) The molecular surface package. *J. Mol. Graphics 11*, 139−141.
(41) *The PyMOL Molecular Graphics System*, version 1.3r1 (2010) Schrödinger, LLC, Portland, OR.
(42) Pettersen, E., Goddard, T., Huang, C., Couch, G., Greenblatt, D., Meng, E., and Ferrin, T. (2004) UCSF Chimera–A visualization system for exploratory research and analysis. *J. Comput. Chem. 25*, 1605−1612.
(43) Batsanov, S. S. (2001) Van der Waals radii of elements. *Inorg. Mater. 37*, 871−885.
(44) Gulick, A. M., Starai, V. J., Horswill, A. R., Homick, K. M., and Escalante-Semerena, J. C. (2003) The 1.75 Å crystal structure of acetyl-CoA synthetase bound to adenosine-5′-propylphosphate and coenzyme A. *Biochemistry 42*, 2866−2873.
(45) Wu, R., Reger, A. S., Lu, X., Gulick, A. M., and Dunaway-Mariano, D. (2009) The mechanism of domain alternation in the acyl-adenylate forming ligase superfamily member 4-chlorobenzoate: coenzyme A ligase. *Biochemistry 48*, 4115−4125.
(46) Crosby, H. A., Pelletier, D. A., Hurst, G. B., and Escalante-Semerena, J. C. (2012) System-wide studies of *N*-lysine acetylation in *Rhodopseudomonas palustris* reveal substrate specificity of protein acetyltransferases. *J. Biol. Chem. 287*, 15590−15601.
(47) Gardner, J. G., Grundy, F. J., Henkin, T. M., and Escalante-Semerena, J. C. (2006) Control of acetyl-coenzyme A synthetase (AcsA) activity by acetylation/deacetylation without NAD(+) involvement in *Bacillus subtilis*. *J. Bacteriol. 188*, 5460−5468.
(48) Du, L., He, Y., and Luo, Y. (2008) Crystal structure and enantiomer selection by D-alanyl carrier protein ligase DltA from *Bacillus cereus*. *Biochemistry 47*, 11473−11480.
(49) Rowland, R. S., and Taylor, R. (1996) Intermolecular nonbonded contact distances in organic crystal structures: Comparison with distances expected from van der Waals radii. *J. Phys. Chem. 100*, 7384−7391.
(50) Xun, L. (2012) Microbial Degradation of Polychlorophenols. In *Environmental Science and Engineering* (Singh, S. N., Ed.) Vol. *14*, pp 1−30, Springer, New York.
(51) Flanagan, P. V., Kelleher, B. P., and Allen, C. C. R. (2014) Assessment of anaerobic biodegradation of aromatic hydrocarbons: The impact of molecular biology approaches. *Geomicrobiol. J. 31*, 276−284.
(52) Lauby-Secretan, B., Loomis, D., Grosse, Y., Ghissassi, F. E., Bouvard, V., Benbrahim-Tallaa, L., Guha, N., Baan, R., Mattock, H., and Straif, K. (2013) Carcinogenicity of polychlorinated biphenyls and polybrominated biphenyls. *Lancet Oncol. 14*, 287−288.
(53) Passatore, L., Rossetti, S., Juwarkar, A. A., and Massacci, A. (2014) Phytoremediation and bioremediation of polychlorinated biphenyls (PCBs): State of knowledge and research perspectives. *J. Hazard. Mater. 278*, 189−202.
(54) Nawarathne, I. N., and Walker, K. D. (2010) Point mutations (Q19P and N23K) increase the operational solubility of a 2 *α*-*O*-benzoyltransferase that conveys various acyl groups from CoA to a taxane acceptor. *J. Nat. Prod. 73*, 151−159.
(55) Ajikumar, P. K., Xiao, W. H., Tyo, K. E. J., Wang, Y., Simeon, F., Leonard, E., Mucha, O., Phon, T. H., Pfeifer, B., and Stephanopoulos, G. (2010) Isoprenoid pathway optimization for Taxol precursor overproduction in *Escherichia coli*. *Science 330*, 70−74.
(56) Jeya, M., Kim, T. S., Tiwari, M. K., Li, J., Zhao, H., and Lee, J. K. (2012) The *Botrytis cinerea* type III polyketide synthase shows unprecedented high catalytic efficiency toward long chain acyl-CoAs. *Mol. BioSyst. 8*, 2864−2867.
(57) Yu, Z.-L., Liu, J., Wang, F.-Q., Dai, M., Zhao, B.-H., He, J.-G., and Zhang, H. (2011) Cloning and characterization of a novel CoA-ligase gene from *Penicillium chrysogenum*. *Folia Microbiol. 56*, 246−252.

DOI: 10.1021/acs.biochem.5b00899
Biochemistry 2015, 54, 6230−6242